Optical Design of the FUV Spectrographic Imager for the IMAGE Mission

Serge Habraken[a], Claude Jamar[a], Pierre Rochus[a]
Stephen Mende[b], and Mike Lampton[b]

[a]Centre Spatial de Liège, Av. du Pré-Aily, B-4031 Angleur (Belgium)
[b]Space Sciences Laboratory, University of California / Berkeley,
Centennial Drive at Grizzly Peak Blvd., Berkeley, CA 94720-7450

ABSTRACT

This paper describes the original concept and the optical design of the IMAGE Mission FUV Spectrographic Imager (SI). The instrument goal is to spectrally separate and image the electron and proton auroras. A 30 Å (3 nm) spectral resolution is required to isolate the electron auroras (1356 Å). The proton aurora imaging requires to efficiently mask the geocoronal Lyman-alpha line (1216 Å), in order to image the Doppler shifted Lyman-alpha light (1217-1223 Å).
A classical SI combines a telescope with a spectrometer. Our SI is consisting of a reverse combination :
(1) a multi-slits Wadsworth monochromator designed to spectrally isolate the two bandwidths (electrons and protons auroras),
(2) a two mirror imager with a crossed delay line detector producing the final imaging on each spectral channel.

Keywords: Monochromator, Spectrograph, Optical design, Aurora

1. INTRODUCTION

The FUV system is an experiment which forms part of the instrument package of the IMAGE program, a NASA/MIDEX mission due for launch in 2000. The FUV system consists of four major subassemblies, namely, a Spectrographic Imager (SI), a Wideband Imaging Camera (WIC), a geocorona (and sun) sensor, and a Main Electronic Package (MEP).

Science requirements driving FUV SI design are :
(1) to image the entire aurora oval from a spinning spacecraft at 7 R_E apogee altitude,
(2) to separate spectrally the statistical noise of the intense, cold geocorona (Lyman-α emissions at 1216 Å) from the hot proton precipitation (Doppler shifted Lyman-α emissions),
(3) to separate spectrally the electron (1304 and 1356 Å) and proton (1216 Å) auroras.

First requirement involves a large field of view : 15° x 15°.
Second requirement gives rise to a high spectral resolution, better than 2 Å. The Doppler shifted Ly-α signal to be detected is about 100 times less intense than the Lyman-α geocoronal emissions at 1216 Å :
→ very low scattering is required to fulfil the spectral resolution
→ slit geometry has to be optimised to give rise to the highest sensitivity.
Third requirement means that the 1356 Å signal must be isolated from the 1304 Å signal : spectral resolution : 30 Å
Nitrogen emissions near 1200 Å (triplet lines at 1199.55, 1200.22, and 1200.71 Å) have also to be filtered out.
The spatial resolution requirement specifies that, from 7 earth radii, the aurora oval shall be imaged with a 90 km x 90 km resolution. The related angular resolution is about 7 arcmin x 7 arcmin i.e. 128 pixels x 128 pixels.
As a summary, the instrument design shall have a higher priority to optimise the spectral behaviour, than the imaging quality.

Two different optical configurations were investigated, in order to fulfil those requirements.
First, a classical configuration : a telescope combined with a spectrometer. [1-4]
Second, a reverted configuration : a monochromator is combined with an imager. The aim of this paper is to present the design of the second type of SI, which was actually selected for the IMAGE Mission.

Further author information -
S. Habraken (correspondance): Email: shabraken@ulg.ac.be; Tel: +32 4 367 66 68; Fax: +32 4 367 56 13
S. Mende: Email: mende@sunspot.ssl.berkeley.edu; Fax: 1 510-643-8302

2. OPTICAL DESIGN DESCRIPTION

2.1. Instrumental Configuration

The instrument consists of two main optical subsystems : a monochromator, and two imagers (one at 1218 Å, the other one at 1356 Å).
Since the FUV mirror reflectivity is critical, our design goal was to reduce as possible the number of optical surfaces.
The monochromator part of the instrument was first designed as simple as possible : a Rowland configuration was considered. Aberrations were too high to fulfil the requirements. Large astigmatism is not the most critical aspect, since the exit slit focus can be optimised to fit with the tangential focus :
→ the image of a pinhole source located at the entrance slit plane is a narrow line, parallel to the exit slit
→ the resulting spectral selectivity will not be affected.
However, coma over a 36 mm height slit on a concave grating with 500 mm radius of curvature was responsible for the bad results. Larger radius of curvature was not allowed due to lack of space available on the spacecraft deck. Since the sensitivity of the instrument is one of the critical aspects, smaller slit height was not investigated .
A Wadsworth configuration [5] requires one more mirror but smaller aberrations are expected. [6]
The monochromator is designed to produce the largest dispersion, in order to reach the required high spectral resolution. Space availability induces a 500 mm maximum focal length baseline. Grating manufacturing leads to a 3600 lp/mm ruling (holographic recording). Figure 1 shows the Wadsworth monochromator ray-tracing. For manufacturing reasons, the radii of curvature of the concave grating and the collimator is imposed at 1000 mm. The grating curvature is spherical; for best slit imaging quality, the collimator curvature is hyperbolic.
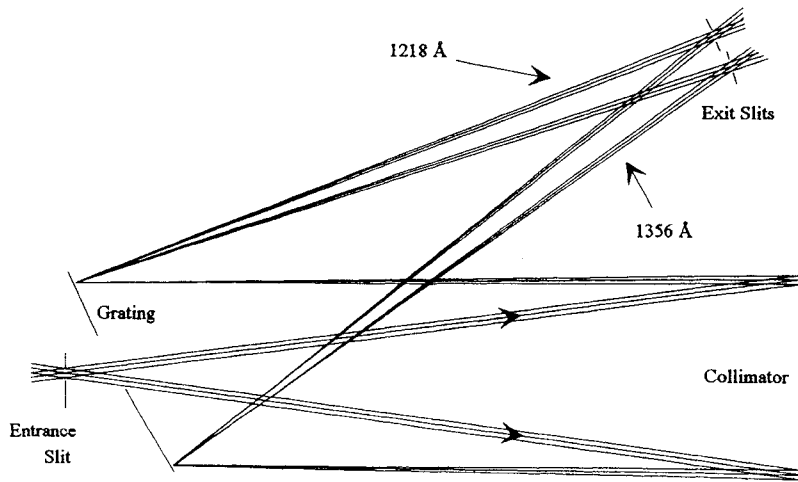

Figure 1 : Wadsworth monochromator : configuration and ray-tracing

This instrument has to efficiently stop the 1200 and 1216 Å lines while transmitting the largest bandwidth in the region from 1217 to 1223 Å, approximately.
The grating angle and the collimator conic constant are optimised to minimise aberrations at 1210 Å i.e. between the 1200 and 1216 Å lines. The 1304 Å blocking is expected to be less efficient. Anyway, since the spectral resolution requirement is much larger at 1356 Å, it can easily be fulfilled.
The linear dispersion is about 182 μm/Å in the exit slit plane. For a 2 Å spectral resolution, the exit slit width would be about 360 μm. The entrance slit width would be (anamorphic magnification : 1/cos(grating angle)) about 400 μm. A compromise between throughput and aberrations level drove the entrance slit height to 36 mm.
The Wadsworth monochromator is highly astigmatic. At the tangential focus the PSF is a thin line, parallel to the exit slit. Spectral performances are related to the width of that PSF line, not its length. For this reason, the astigmatism doesn't need to be corrected.

Paragraph 2.2 will detail a multi-slit configuration, adopted to improve the throughput of the instrument.

As depicted in figure 1, a first image is produced approximately at the grating plane (focus of the beams, after reflection on the so-called 'collimator' mirror. The aim of both imagers is to relay this image after diffraction by the grating, in order to obtain two spectrally separated images.

For ease of manufacturing, two identical imagers are used : one is working at 1218 Å, the other one is working at 1356 Å. Each imager is a two mirrors optical system. The first mirror is spherical. The second one is conical (elliptical) and off-axis. The two imagers are perfectly symmetric (only the back focal length is slightly different, due to geometry difference in the intermediate image to be relayed). So, two identical spherical, and two identical conical mirrors will be manufactured. A flat folding mirror is added on the 1356 Å imager in order to allow fitting the two detectors in close proximity.
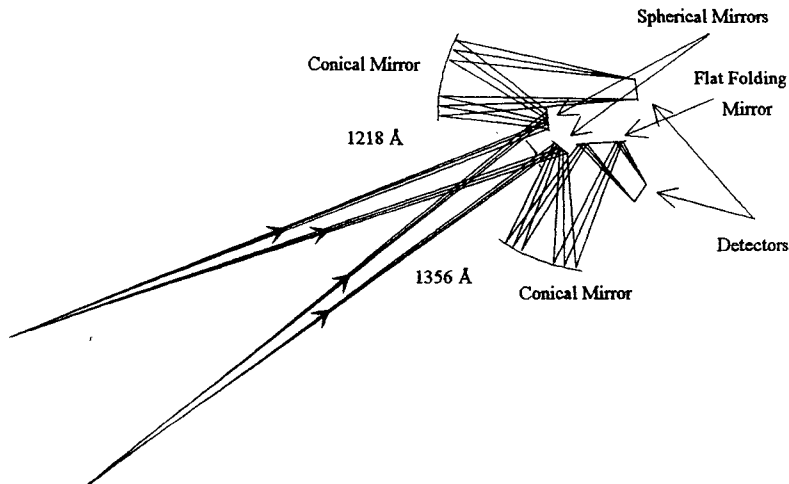
Figure 2 is a sketch of the imagers.

Figure 2 : Back-imagers : configuration and ray-tracing

The imagers are not optimised independently of the Wadsworth monochromator. Astigmatism, that was not critical for spectral selection at the exit slit plane, is now the main aberration to be corrected by the imagers, in order to generate the finest image on the detectors (see § 3.1).

2.2. Optimised Optical Layout

The complete optical layout is shown on figure 3. It combines the monochromator and the two back-imagers. Both image planes are square, approximately 18 x 18 mm².
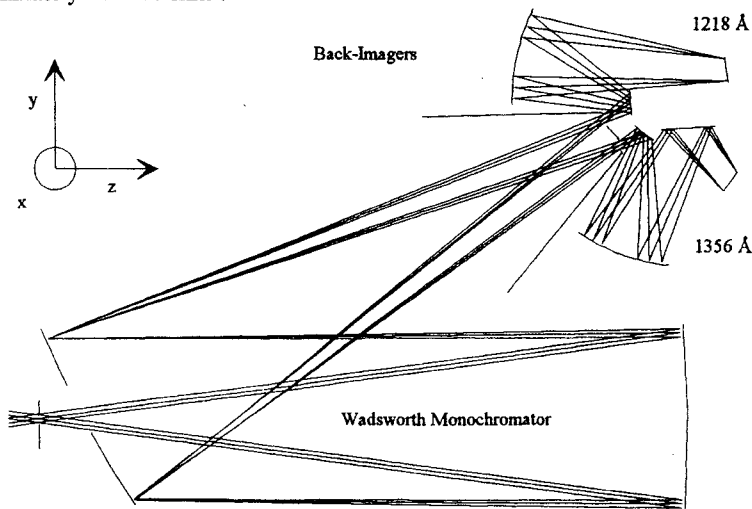

Figure 3 : Configuration and ray-tracing of the SI.

The slit configuration is specifically optimised to enhance the throughput : a grill with 9 slits is designed to stop the 1200 and 1216 Å (1215.67 Å) lines, simultaneously. The slit spacing (period) is determined for this purpose : 5.223 Å i.e. one third of the wavelength difference between the two lines. The 1200 and 1216 Å images of the slits, at the exit slit plane, are perfectly superposed : the image of first slit at 1216 Å is superposed to the image of the fourth slit at 1200 Å. Due to the off-axis configuration of the Wadsworth, the exit slit image is slightly distorted (radius of curvature : ~1300 mm). Since the effect of such a curvature on a 36 mm slit is not negligible, a curved slit grill shall be manufactured. The slit width was optimised, compromising the throughput and the blocking efficiency. The present geometry specifies 1.9 Å wide slits, with masks (or bars) between slits 3.323 Å wide. The focus plane and tilt of the exit slit assembly are optimised at Lyman-α.

The actual dimensions of the entrance slits are related by the linear dispersion and the anamorphic magnification :

$$W(\mu m) = \frac{A}{\cos(\alpha)} \Delta\lambda(\text{Å})$$ [1]

where   A is the linear dispersion = 182 μm/Å ,
α is the grating angle = 28°.

The slit width becomes 391.6 μm.

The exit slit grill do not require the anamorphic correction, but a tilt correction due to the tilt of the exit slit plane. The exit slit width is 356.5 μm.

2.3. Optical Specifications

A grill with 9 parallel, equally spaced, and identical slits was designed. Figure 4 details the slit specifications and geometry, according to the explanations from paragraph 2.2.

Table 1 lists the specifications of optical parts of the SI.
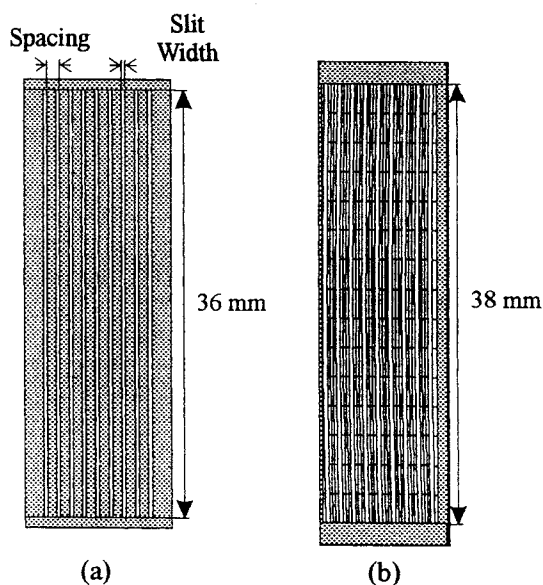
Slit width :   1.9 Å
Bar width :   3.323 Å
Slit spacing :   5.223 Å
Linear dispersion : 182 μm/Å.

	Entrance slits	Exit slits
Slit width (μm)	391.6	356.5
Spacing (μm)	1076.6	980.1
Curvature	no	R = 1300 mm

Figure 4 : Slits geometry. (a) : entrance slits   (b) : exit slits

	Radius of curvature (mm)	Conic Constant	Off-set (mm)	Size (mm)	
				x	y
Collimator Mirror	1000 (concave)	-1.727	0	181	156
Grating	1000 (concave)	0	0	142	164
Spherical Mirrors	136.461 (convex)	0	0	52	20.25
Conical Mirrors	170.725 (concave)	0.114	53.5	144	76
Flat 1356 Å	-	-	-	72	45.5

Table 1 : Optical specifications of the elements.

The coordinate system is (see figure 3):

- z-axis : along the incident light (FOV = 0°),
- x-axis : along the entrance slits height,
- y-axis : along the entrance slits width ('spectral-axis').

The grating central cut-out hole is specified after an analysis of the second order ghost blocking (see § 3.3). Since an image is first produced at the grating plane (approximately), the grating hole induces a blind area on the final image (detector planes).

The focal length of the SI is about -81 mm (small differences appear between the two imagers).

Since the entrance aperture is 9 mm x 36 mm, The F# is :

$$F\#_x = 2.25 \quad \text{and} \quad F\#_y = 9 \tag{2}$$

Since the image is about 18 x 18 mm², corresponding to a square FOV 15° x 15°, the spatial resolution (128 x 128 pixels²) can easily be deduced :

The imaging requirement was defined as : HEW within 1 pixel, and 1 pixel is 7 arcmin. x 7 arcmin.

The related spatial extent on the detector shall be 140 μm x 140 μm (18 mm/128).

So, the imaging requirement is HEW smaller than 140 μm (1 pixel).

3. OPTICAL DESIGN VERIFICATION

3.1. Imaging Performances

The SI configuration is quite unusual. It gives rise to surprising spot diagram at the detector plane (see Figure 5), with non axi-symmetric Point Spread Function (PSF). The calculation of Encircled Half Energy Width (HEW) sometimes suffers from a lack of significance.
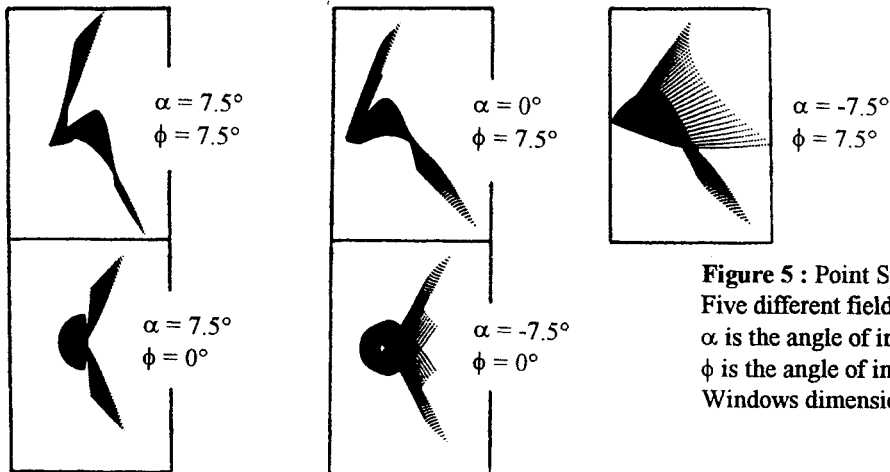

α = 7.5°
φ = 7.5°

α = 0°
φ = 7.5°

α = -7.5°
φ = 7.5°

α = 7.5°
φ = 0°

α = -7.5°
φ = 0°

Figure 5 : Point Spread Function (PSF) at 1218 Å.
Five different fields of view are shown.
α is the angle of incidence, into the y-z plane
φ is the angle of incidence, into the x-z plane.
Windows dimensions : 300 μm x 200 μm

The HEW never exceed 135 μm. The average value, over the whole FOV, is about 120 μm. The same results appear at 1356 Å. We conclude that the imaging performances are within the specifications, with a small margin for manufacturing and thermal tolerancing.

3.2. Spectral Filtering Performances

The optimised slit geometry is depicted by figure 4.

The spectral filtering of the monochromator is directly related to the slit imaging quality. As already mentioned, the image is highly astigmatic.

The best focus is the tangential focus :   - large PSF parallel to the slit (x-axis)
                                                - narrow PSF perpendicular to the slit (y-axis)

Figure 6 depicts the slit imaging of the Wadsworth monochromator at 1216 Å: Each entrance slit is filled with 20 sources, along the height. 5 slits are shown (1st, 3rd, 5th, 7th, and 9th). The image of each source is a single line with RMS size about 18 μm at the slit centre (x = 0) and 70 μm at the slit edges (x = ±18 mm) (for any slit, from the 1st to the 9th).

The imaging quality is worse at 1200 Å : RMS size about 200 μm at the slit centre (x = 0) and 130 μm at the slit edges (x = ±18 mm). The spectral filtering will be significantly affected (see figure 8).

548

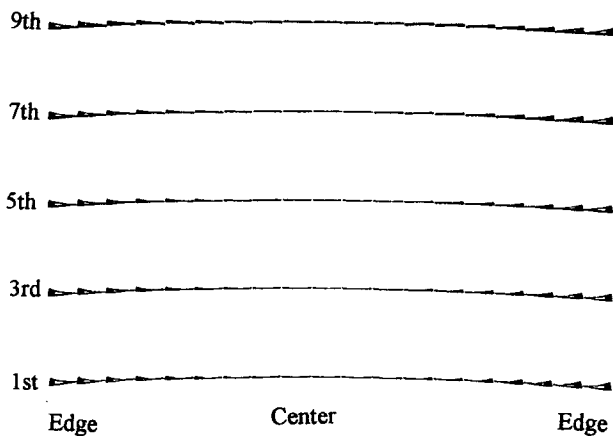9th

7th

5th

3rd

1st

Edge   Center   Edge

Figure 6 : slit imaging of the Wadsworth monochromator at 1216 Å. Each entrance slit is filled with 20 sources, along the height. 5 slits are shown.
Drawing not in scale (spectral axis enlarged).
The slit curvature is also depicted.

Ray-tracing was performed to evaluate the spectral filtering (or blocking) performances of the Wadsworth monochromator. The above calculations do not take into account the scattering level of the reflective surfaces (collimator and grating) as well as diffraction effects due to slit apertures.

The exit slit position was optimised, according to the fact that the 1200 Å lines (1199.55, 1200.22, and 1200.71 Å) are not as intense as the L_α line (1215.67 Å). It was specified that the 1200 Å lines should never exceed 10% transmission.

The filtering quality is summarised on table 2, and figures 7-9 :

Wavelength (Å)	Transmission (%)
1199.55	3.6
1200.22	0.65
1200.71	5.5
1215.67	0
1218.2	93
1220.9	0
1223.5	77
1226	0.1

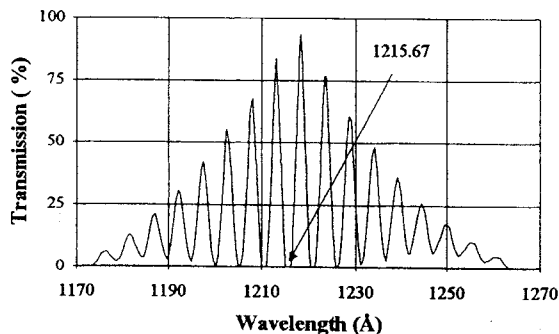**Table 2** : Filtering quality of the monochromator with the optimised slit grill.

Figure 7 : Spectral filtering of the exit slit grill.

Figure 8 : Spectral filtering performances in the 1200 Å region.
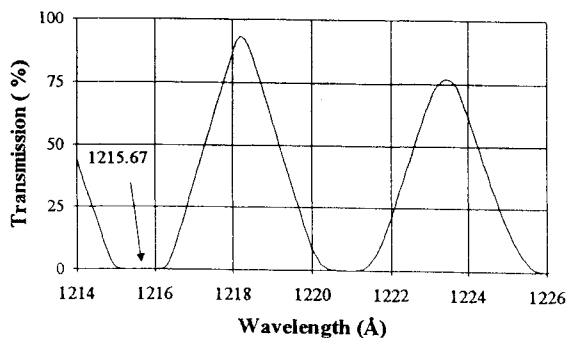

Figure 9 : Spectral filtering performances in the 1216 Å region.

These figures demonstrate that the instrument is efficiently stopping the unwanted rays.

3.3. Stray Light Analysis

Stray-light sources that we have to take into account are :
1. Direct light from outside the spectrometer towards the exit slits, at any wavelength.
2. Grating zero order, at any wavelength.
3. Light from other diffraction orders, at a selection of critical wavelengths.
4. Light due mainly to scattering of the collimator and the grating.

The stray light reduction is performed by different methods (see figure 10):
→ Black anodization of all parts.
→ The imager is isolated (light tightness only) from the Wadsworth monochromator by a specific screening. Only the exit slits may transmit light from the monochromator to the imager zone.
→ A baffle is located in front of the entrance slits, attached to the front door assembly. The front door assembly itself is designed with vanes that reduces the unobstructed field of view (UFOV).
→ Baffling with vanes to efficiently trap the zero order.
→ Except from the zero order, in the visible domain, the grating do not produce any diffraction order (evanescence).
→ If 250 nm < λ < 400 nm, the +1 order of the grating is illuminating vanes depicted at figure 10 (at the bottom). Those vanes are designed to produce the required reduction.
→ If 230 nm < λ < 250 nm, the +1 order is reflected back and, finally, passes through the grating hole (Littrow mounting).
→ If λ < 230 nm, several orders (-1, 0, +1, +2) with several directions (according to the wavelength) are presents. Vanes design is optimised for such a purpose.
→ Collimator and grating with low scattering level are required (RMS roughness better than 10 Å).
Figure 10 shows a ray-tracing at 1218 and 1356Å including the zero and +1 diffraction orders only (for clarity). The depicted model of the FUV-SI was used to optimise the stray light reduction, with the ASAP software.
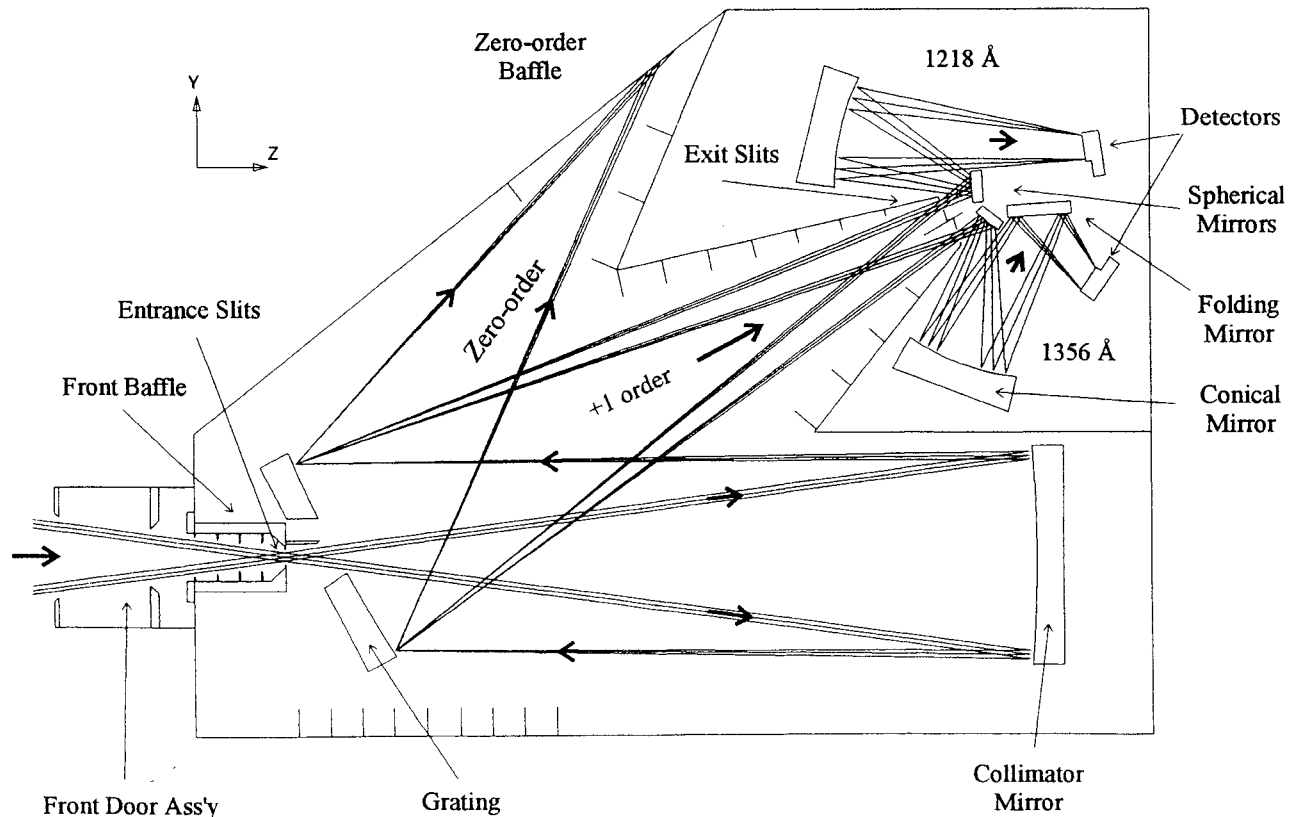

Figure 10 : Ray-tracing at 1218 and 1356Å including the zero and +1 diffraction orders.
Stray-light model of the FUV-SI optimised with the ASAP software.

The basis of the stray light analysis of this instrument is simple. Since an intermediate image is produced near the grating, any rays that could be scattered around the grating, towards exit slits, is a stray light source. So, great care shall be required during the design of the grating mounting bracket.

The visible light rejection goal is 10^{-9}. We assume only anodised surfaces. The design shown on figure 10 reaches the required performances at any FOV in the visible and near UV spectrum. FUV specifications require to efficiently block several emission bands. Figures 7-9 show the light reduction expected with the slit configuration from figure 4.

The Oxygen emission around 1304 Å has also to be reduced below 1 %. No direct light is transmitted through any of the exit slits (1304 Å light is directed towards an area located between the 1218 and 1356 Å slits). Stray light is well below 1 %. But multi-reflection/diffraction of the second diffraction order is responsible for ghost imaging at 1304 Å on both detectors. This image results from a double diffraction from the grating : light is first 2nd-order diffracted, travelling back to the collimator. After reflection, light is +1-order diffracted towards the exit slits. The effect is observed only for small FOV.

We demonstrated that a small increase of the grating cut-out hole size can totally suppress the second order ghost imaging : larger central hole (decentered) induces that light is now travelling back through the hole, instead of being diffracted by the grating.

Then, the required grating hole is 50 mm x 44 mm = 2200 mm^2 (9.5 % of the total grating surface).

Location of the hole : relation to the centre of the grating,

> x-axis : ± 25 mm   y-axis : -13, +31 mm

Therefore, the related FOV defines a blind rectangle inside the full FOV (15° x 15°) with

> ϕ : -2.9°, 2.9°   and α : -1.35°, 3.2°

3.4. System Transmittance

One of the driver of the instrument design is the search for the highest throughput which naturally induces an optical configuration minimising the number of reflective surfaces.

At 1218 Å, light is reflected 4 times, diffracted (first order) by the grating, and transmitted by the exit slits.

If we assume a Ly-α optimised mirror coating (Al-MgF$_2$), the expected reflectivity is about 75 % , [7] for each mirror.

The diffraction efficiency of a sinusoidal grating is about 30%.

The transmission of light through the exit slit grill is about 90%, in the 1218 Å region (see table 2).

We deduce that the overall transmission of the system is 8.5%.

3.5.   Tolerancing

3.5.1. Positioning Tolerances and adjustment requirements

Since the instrument has to be aligned mainly by FUV light, it shall be operated under vacuum. Consequently, adjustment capabilities need to be motorised. The tolerancing budget has to minimise the adjustment requirements : when tolerances are large enough to be reached by precision machining, no adjustment is foreseen.

No adjustment of the exit slits is needed, if the entrance slits can be accurately adjusted. Since the L$_\alpha$ stopping is the most critical part of the alignment, the y-decenter motion and the slit roll will be adjustable. The focus (z-axis) is fixed (adjustment capability lead on the collimator). Positioning accuracy of the image at exit slit 1356 Å get much larger tolerances. Once the exit slit grill is aligned, the 1356 Å slit is aligned with enough accuracy, by mechanical manufacturing. The collimator focus provides an efficient tool to correct the slit imaging for a wrong collimator and/or grating radius of curvature. So, large motion of the collimator is desirable (several mm) to correct the radius of curvature, enlarging the radius tolerance.

A a grating tilt (yaw) is needed to correct a wrong grating spatial frequency, enlarging grating period tolerance.

The imager positioning is tolerant towards the monochromator . Inside the imager, relative positioning between spherical and conical mirrors is very tight. As a matter of fact, most of the spherical mirror positioning errors can be corrected by an adjustment of the conical mirror ! Since the space around the spherical mirrors is minimal, these mirrors will stay fixed.

The performance is very sensitive with respect to the distance between spherical and conical mirrors : correction is accomplished by means of the conical mirror focus adjustment. Since the conical mirrors are off-axis, they are very sensitive to decentering in the y-axis (off-set error). Specific adjustment procures correction capability for spherical mirror yaw tolerance and conical mirror manufacturing tolerances (off-set error).

Since the refractive index of the detector MgF$_2$ window is not precisely defined, an adjustment of the detector focus is required. It is also provided by the conical mirror focus.

As demonstrated, we have carefully selected adjustments in order to simplify alignment tools.

3.5.2. Production Tolerances

As discussed in the above paragraph, tolerances are related to adjustment capabilities.
Table 3 summarises the acceptable fabrication tolerances of the optics.

Element	Specifications		Tolerances		
	Radius (mm)	Conic constant	Radius (mm)	Conic constant	Irregularity (fringes at 633 nm wavefront, RMS)
Collimator	1000	-1.727	5	0.02	2
Grating	1000	0	5	-	1
Spherical mirrors	136.461	0	0.25	-	1
Conical mirrors	170.725	0.114	0.3	0.005	2
Flat Folding mirror	∞	0	-	-	2

Grating : spatial frequency tolerances : 3600 lp/mm ± 10 lp/mm

Table 3 : Summary of optics fabrication tolerances.

3.5.3. Thermal Tolerances

An aluminium (α = 23.8 10^{-6} /m/°C) base plate is assumed.
The thermal range for optical quality is highly related to the expansion coefficient of the mirror blank : the best system would consist in full aluminium mirrors. Since we require a super-polishing of the monochromator mirrors (10 Å RMS micro-roughness), this solution is not adequate. We intend to use BK7 glass (α = 7.1 10^{-6} /m/°C) for the collimator and NG5 glass (α = 6.5 10^{-6} /m/°C) for the grating (absorptive glass allowing holographic recording through a lightweighted substrate).
The thermal variation on the S/C platform is expected to be ±20°C.
Ray-tracing simulations were performed :
→ Positioning of elements is affected according to the Aluminium base plate expansion.
→ Mirror radii of curvature are changing according to the glass substrate thermal properties.
→ Fringe spacing of the grating is expanded by the same amount as the NG5 glass substrate.
Figures 11 and 12 show the thermal variation impact on the Wadsworth monochromator.
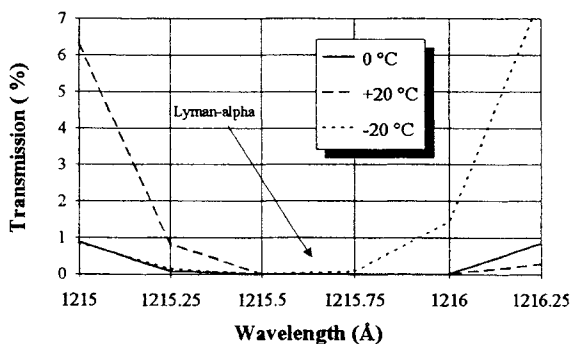The residual transmission at the two critical wavelengths is depicted : 1200 and 1216 Å.

Figure 11 : Thermal variation impact on the mono-
chromator spectral selectivity, around 1216 Å : dT = 0°C is
the temperature of the alignment procedure. The residual
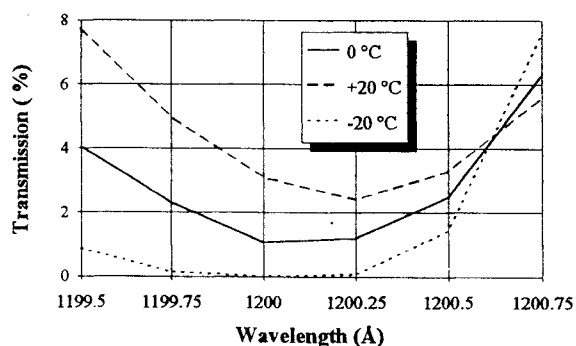transmission vs. wavelength is plotted at 3 different dT.

Figure 12 : Thermal variation impact on the
monochromator spectral selectivity, around 1200 Å.

The spectral behaviour suffers from the thermal misalignment, but figures 11 and 12 show that a 20°C variation is still acceptable. Thermal gradients were also simulated within the same thermal range. The same conclusion applies.

The imaging quality, at the detector plane, is not highly related to a Wadsworth misalignment : to some extent, the imager assembly is separated from the monochromator assembly. Since only conical mirrors are not aluminium, thermal degradation is significantly reduced. Variations of the RMS spot size are between 0.2 and 0.5 µm/°C.

4. CONCLUSIONS

This paper described how requirements and specifications of the FUV Spectrographic Imager for the IMAGE Mission are fulfilled by optical design . Imaging and spectral performances are optimised. Opto-mechanical and thermal tolerances are investigated. Adjustment provisions are minimised by careful selection. A summary of the stray-light analysis is presented. The reverted configuration (Monochromator + imager) permits to optimise a slits grill with a very efficient Lyman-α rejection. A classical design (telescope + spectrometer) was first investigated. Reasons why it was not selected are :

→ the maximum number of slits (for proton aurora imaging, 1218 Å) was three, instead of nine.

→ no Ly-α rejection was performed : on the detector, the Ly-α image was shifted close to the proton aurora image (2 Å resolution ⇨ ± 350 μm spacing, on the detector). Stray light effects and detector range were of concern.

So, for its spectral filtering quality and high throughput, the reverted configuration was selected.

This configuration could also apply with a Rowland, instead of a Wadsworth mounting when the slit height/focal length is not a critical parameter for the design. Indeed, smaller slit height and/or larger grating radius of curvature decrease significantly the coma aberration.

REFERENCES

1. T. E. Berger and alv., "HIRES: High Resolution Extreme-Ultraviolet Spectroheliometer : toroidal diffraction grating performance evaluation," *Ultraviolet Technology IV*, SPIE proc. **1764**, pp. 218-230, 1992.

2. M. C. Huber and G. Tondello, "Stigmatic performance of an EUV spectrograph with a single toroidal grating," Appl. Opt. **18**(23), pp. 3948-3953, 1979.

3. H. Rippel, D. Kampf, and R. Graue, "ORFEUS : Orbiting and Retrievable Far and Extreme Ultraviolet Spectrometer," *EUV Optics for astronomy, Microscopy, Polarimetry, and Projection Lithography*, SPIE proc. **1343**, pp. 520-529, 1990.

4. M. E. Gangl, J. H. Middlestadt, and R. W. Eastes, "AURA, an experiment to measure ultraviolet radiation of the Earth's atmosphere from space," *Ultraviolet Technology IV*, SPIE proc. **1764**, pp. 50-60, 1992.

5. M. Seya and T. Namioka, "Theory of the Wadsworth Mounting," Sci. of Light **16**(2), pp. 158-168, 1967.

6. H. G. Beutler, "The theory of the concave grating," J. Opt. Soc. Am. **35**(5), pp. 311-350, 1945.

7. Acton Research Corporation (AR_C), Al+MgF$_2$ coating ARC #1200 : expected reflectivity > 80% at 120-140 nm.